

Comment on acp-2022-26 titled "Review of "The impact of atmospheric motion on source-specific black carbon and the induced direct radiative effect over a river-valley region" by Liu et al.

Anonymous Referee #2

General comment

The site location should be described in more detail, and also earlier on. Some more comments on this issue are below.

Response: We have taken the suggestion to heart and have added more details about the location description. The revised site description now reads:

“Baoji is a typical river-valley city, located at the furthest west of the Guanzhong Plain, at an altitude from 450 to 800 m a.s.l. (Figure S1), Baoji has a complex topography and often suffering from severe pollution in winter. It is surrounded by mountains to the south, west and north, with the Weihe River as the central axis extending eastward. The shape can be viewed as a funnel, with large opening to east. The Qinling peaks and the flat Weihe Plain are the main landforms of Baoji. The main peak of the Qinling Mountains is 3,767 m a.s.l. and it is the highest mountain in the eastern part of mainland China. This terrain causes divergent flow at local scales, which can impact pollution levels (Wei et al., 2020). Baoji also is an important railway intersection in China, connecting six railways to the north-west and southwest China. Pollutant levels can be high and pollutants are not easy to be dispersed in the city due to its special topographic conditions, dense population (total population of 0.341 million, with 63.5% population living in the downtown area and population density of 6003 people per km² in 2019 (<http://tjj.shaanxi.gov.cn/upload/2021/zk/indexch.htm> and <https://data.chinabaogao.com/hgshj/2021/042053X932021.html>), and impacts from major highway and railway networks.

The sampling site was on the rooftop of a building at Baoji University of Arts and Sciences (34°21'16.8"N, 107°12'59.6"E, 569 m a.s.l.) surrounded by commercial and residential buildings, highways, and a river, there were no major industrial emission sources nearby. The main sources of BC in Baoji were the domestic fuel (coal and biomass) burning as well as the motor vehicle emissions (Zhou et al., 2018; Xiao et al., 2014). Open fire also can be sources for BC, but there were limited fire found scattered around the site (Figure S2). The meteorological conditions at Baoji for the four seasons are listed in Table S1, and the wind roses for the different seasons are shown in Figure S3(data are from the Meteorological Institute of Shaanxi Province).”

Table R1 The seasonal meteorological data of Baoji

| Season | Temperature (°C) | Relative humidity (%) | Precipitation in last hour (mm) |
|--------|------------------|-----------------------|---------------------------------|
| Winter | 2.7 | 60.6 | 0.025 |
| Spring | 11.5 | 54.9 | 0.042 |
| Summer | 23.7 | 67.1 | 0.139 |
| Autumn | 20.2 | 67.0 | 0.074 |

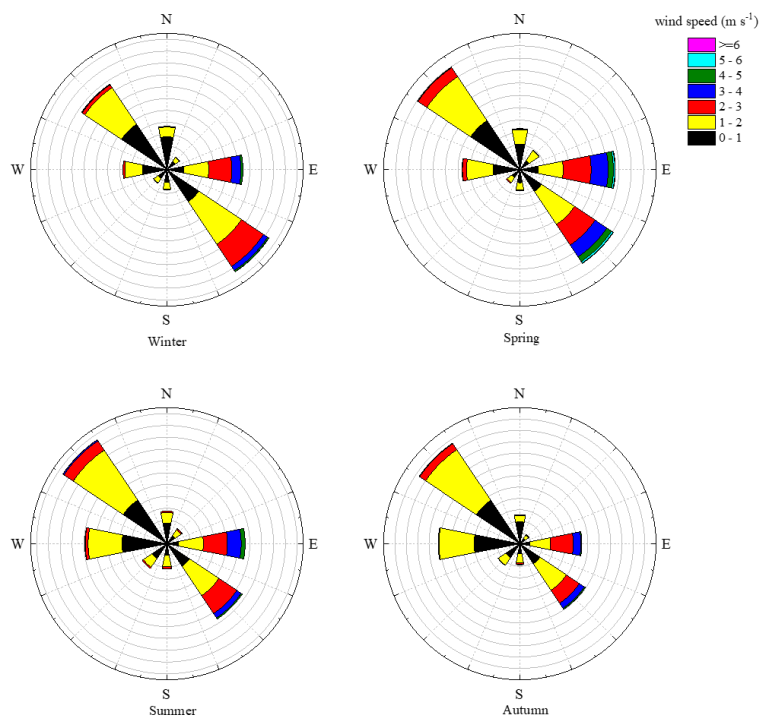


Figure R1 Seasonal wind roses for Baoji.

The English grammar and style could be quite significantly improved. A few examples of some issues are provided in the specific comments below, but many more instances are present in the paper. Maybe some editorial work by a native-speaking scientist could help improve the language and therefore clarity.

Response: Thanks for pointing out those grammatical mistakes in the specific comments and as suggested we had the paper polished by a native English speaker.

The origin of the biomass burning BC is not well described or discussed. Is this agricultural biomass burning, wildfires, or residential biomass burning? Something else?

Response: The field sampling happened in winter (from 16th November 2018 to 21st December 2018), in Baoji wildfires were comparatively sparser, we screenshotted the fire map (data from MODIS/Aqura, MODIS/Terra and VIIRS 375m/Suomi NPP) from NASA, as shown in Figure R2. Although China has banned agriculture biomass burning due to the air pollution, a lack of strict supervision leads to a few illegal burning in rural areas. Biomass (e.g. straw and crop) is one of the common solid fuel for residential heating and home cooking in winter which causes severe air pollution (Wu et al., 2019). Thus, we believe the biomass burning BC could be from all the three sources but residential biomass burning may take the major responsibility. We have added the potential emission sources of BC at study site in the section 2.1 Research site, see the response above.

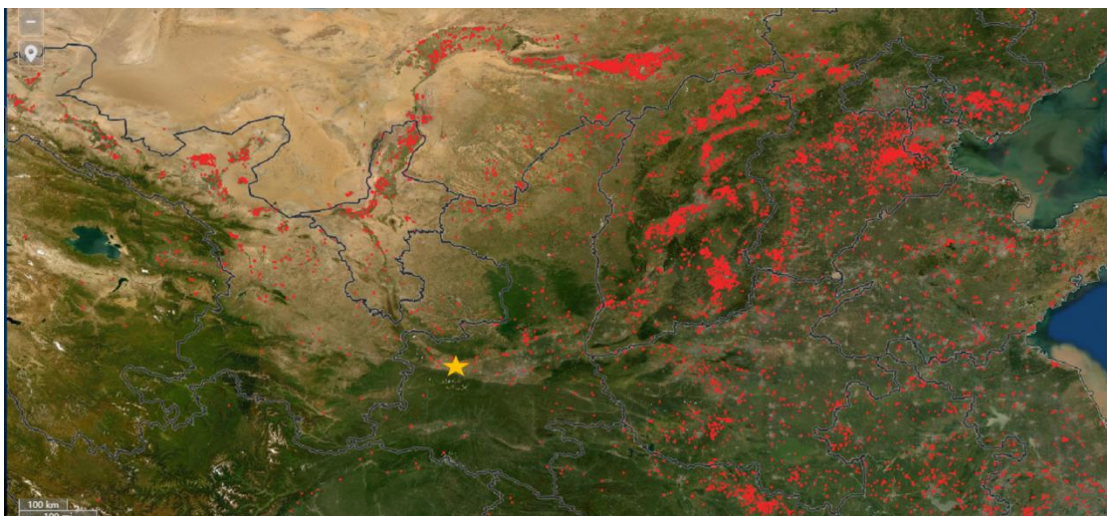


Figure R2. Map of fire occurrences. The yellow star represents the study site, the red dots represent the fire. The image from © NASA (National Aeronautics and Space Administration) (<https://firms.modaps.eosdis.nasa.gov/map>).

Reference:

Wu S., Zheng, X., You, C., and Wei, C.: Household energy consumption in rural China: Historical development, present pattern and policy implication, *Journal of Cleaner Production*, 211, 981-991, <https://doi.org/10.1016/j.jclepro.2018.11.265>, 2019.

The literature citations are a bit scarce and somewhat biased. A broader representation of the work published in the literature and relevant to the authors' work outside of their own work, would help.

Response: We reviewed more studies and replaced some of the research citation from our work. In addition, we added the comparison of studies on BC pollution and the total DRE of BC in other river valley sites. The revised part is shown was following:

“The mean values of eBC_{fossil} and $eBC_{biomass}$ were $2.46 \mu g m^{-3}$ and $1.17 \mu g m^{-3}$, respectively. The averaged total eBC mass concentration (\pm standard deviation) was $3.63 \pm 2.73 \mu g m^{-3}$, and the eBC ranged from varying from 0.39 to $12.73 \mu g m^{-3}$ during the study period, The averaged mass concentration was comparable to that in Lanzhou, another river valley city in China, that was sampled in the same season (5.1 ± 2.1 , Zhao et al., 2019). The lowest value is comparable to other river valley regions such as in Retje in India (Glojek et al., 2022) or in Urumqi River Valley in China (Zhang et al., 2020), however even the highest concentration was much lower than that in other urban regions (Table S5).”

“The $DRE_{eBC, TOA}$ and $DRE_{eBC, SUF}$ of eBC were $13 W m^{-2}$ and $-22.9 W m^{-2}$, which were lower than that reported in Lanzhou ($21.8 W m^{-2}$ and $-47.5 W m^{-2}$ for $DRE_{eBC, TOA}$ and $DRE_{eBC, SUF}$) – which is another a river valley city in China (Zhao et al., 2019). This could be due to fact that the eBC mass concentration in Baoji was lower than in Lanzhou (Table S5). As for the $DRE_{eBC, TOA}$ and $DRE_{eBC, SUF}$ per an unit mass of BC, the results of the two studies were comparable.”

Table R2 Mean (range) BC mass concentration in river valley sites worldwide.

| Reference | BC concentration ($\mu\text{g m}^{-3}$) | Season | Topographic conditions | Altitude | Station type | Year |
|----------------------------|-------------------------------------------|----------------------------|------------------------|---------------------|--------------|-----------|
| This study | 3.63±2.73 (0.39~12.73) | November~December (winter) | river valley | 450 to 800 m a.s.l. | urban | 2018 |
| Glojek et al., (2020) | 0.9~40 | December~January (winter) | river valley | 715 m a.s.l. | rural | 2017-2018 |
| Zhao et al. (2015) | 25±11 | January (winter) | river valley | 410 m a.s.l. | urban | 2013 |
| Barman and Gokhale (2019) | 20.58~22.44 | Winter | river valley | | urban | 2016-2017 |
| Zhang et al., 2020 | 0.102~1.525 | Winter | river valley | 2130 m a.s.l. | rural | 2016-2017 |
| Chakrabarty et al., (2012) | 9~41 | January~February (winter) | river valley | | urban | 2011 |
| Zhao et al. (2019) | 5.1 ± 2.1 | December~January (winter) | river valley | | urban | 2018 |
| Tiwari et al., 2016 | 8.19 ±1.39 | December-February (winter) | river valley | 55 m a.s.l. | urban | 2013-2014 |

Reference:

Barman, N., and Gokhale, S., Urban black carbon - source apportionment, emissions and long-range transport over the Brahmaputra River Valley, *Science of the Total Environment*, 693, 133577, <https://doi.org/10.1016/j.scitotenv.2019.07.383>, 2019

Chakrabarty, R., Garro, M., Wilcox, E., and Moosmuller, H., Strong radiative heating due to wintertime black carbon aerosols in the Brahmaputra River Valley, *Geophysical Research Letters*, 39, L09804, <https://doi.org/10.1029/2012GL051148>, 2012.

Glojek, K., Močnik, G., Alas, H., et al., The impact of temperature inversions on black carbon and particle mass concentrations in a mountainous area, *Atmos. Chem. Phys.*, 22, 5577–5601, <https://doi.org/10.5194/acp-22-5577-2022>, 2022.

Zhang, X., Li, Z., Ming, J., and Wang, F., One-Year Measurements of Equivalent Black Carbon, Optical Properties, and Sources in the Urumqi River Valley, Tien Shan, China, *Atmosphere*, 11, 478, <https://doi.org/10.3390/atmos11050478>, 2020.

Zhao, S., Yu, Y., Yin, D., et al., Concentrations, optical and radiative properties of carbonaceous aerosols over urban Lanzhou, a typical valley city: Results from in-situ observations and numerical model, *Atmospheric Environment*, 213, 470–484, <https://doi.org/10.1016/j.atmosenv.2019.06.046>, 2019.

Zhao, S., Tie, X., Cao, J & Zhang, Q. (2015), Impacts of mountains on black carbon aerosol under different synoptic meteorology conditions in the Guanzhong region, China. *Atmospheric Research*, 164-165, 286-296. <http://dx.doi.org/10.1016/j.atmosres.2015.05.016>

Tiwari, S., Kumar, R., Tunved, P., Singh, S., and Panicker, A., Significant cooling effect on the surface due to soot particles over Brahmaputra River Valley region, India: An impact on regional climate, 2016, Science of the Total Environment, 562, 504–516, <http://dx.doi.org/10.1016/j.scitotenv.2016.03.157>, 2016.

Maybe is my lack of familiarity with some of these aspects, but some of the data analysis methods (e.g., SOM, but not only) are not described in sufficient detail. The authors refer to existing literature, but a brief description of the methods' workings, input, outputs, limitations, etc. would help improve the clarity and broaden the audience of the paper.

Response: We are truly grateful for reviewer's comments and suggestion. We revised the methods to provide more details particularly for the optical source apportionment and SOM. Other methods also have been revised according to the reviewer's suggestions. In addition, we have provided information regarding the cluster analysis and minimum R squared method in the supplementary materials. The changes are shown in the revised version. The revised paragraphs now read as follows:

"2.2 Sampling and laboratory measurements

eBC and the absorption coefficients (b_{abs}) at 370, 470, 520, 590, 660, 880, and 950 nm wavelength were measured using an AE33 aethalometer (Magee Scientific, Berkeley, CA, USA) equipped with a PM_{2.5} cut-off inlet (SCC 1.829, BGI Inc. USA) that had a time resolution of 1 min. A Nafion® dryer (MD-700-24S-3; Perma Pure, Inc., Lakewood, NJ, USA) with a flow rate of 5 L min⁻¹ was used to dry the PM_{2.5} before the measurement. Briefly, the particles were dried by the Nafion® dryer before being measured with the AE33 aethalometer, and the deposited particles were irradiated by light-emitting diodes at seven wavelengths of light-emitting diodes ($\lambda = 370, 470, 520, 590, 660, 880, \text{ and } 950 \text{ nm}$), and the light attenuation was detected. The non-linear loading issue for filter-based absorption measurement was accounted for in the AE33 by a technique called dual-spot compensation. The quartz filter (PN8060) matrix scattering effect was corrected by using a factor of 1.39. More details of AE33 measurement techniques can be found in Drinovec et al. (2015).

The scattering coefficient (b_{scat}) at a single (525) nm wavelength was measured with the use of a nephelometer (Aurora-1000, Ecotech, USA) that had a time resolution of 5 min. The nephelometer and aethalometer operated simultaneously and used the same PM_{2.5} cyclone and Nafion® dryer. The calibration was conducted based on the user guide with a calibration gas R-134. Zero calibrations were conducted every other day by using clean air without particles. The ambient air was drawn in through a heated inlet with a flow rate of 5 L min⁻¹. The relative humidity remained lower than 60%.

PM_{2.5} samples were collected for every 24 hours (h) from 10 a.m. local time to the 10 a.m. the next day from 16th November 2018 to 21st December 2018 with two sets of mini-volume samplers (Airmetrics, USA), one using quartz fiber filters (QM/A; Whatman, Middlesex, UK) and the other with Teflon® filters (Pall Corporation, USA), both with a flow rate of 5 L min⁻¹. Those samples were kept in a refrigerator at 4°C before analysis. The mass concentration of K⁺ in the PM_{2.5} quartz sample was extracted in a separate 15 mL vials containing 10 mL distilled deionized water (18.2 MΩ resistivity). The vials were placed in an ultrasonic water bath and shaken with a mechanical shaker for 1 h to extract the ions and determined by a Metrohm 940 Professional IC Vario (Metrohm AG., Herisau, Switzerland) with Metrosep C6-150/4.0 column (1.7 mmol/L nitric acid+1.7 mmol/L dipicolinic acid as the eluent) for cation analysis. A group of elements (i.e. Mg, Al, Si, S, Cl, Ca, V, Mn, Fe, Ni, Cu, As, Se, Br, Sr, Pb, Ga, and Zn) on the Teflon® filters was determined by energy-dispersive x-ray fluorescence (ED-XRF) spectrometry (Epsilon 4 ED-XRF, PANalytical B.V., Netherlands). The X-rays were generated from a gadolinium anode on a side-window X-ray tube. A spectrum of the ratio of X-ray and photon energy was obtained after 24 minutes of analysis for each sample

with each energy peak characteristic of a specific element, and the peak areas were proportional to the concentrations of the elements. Quality control was conducted on a daily basis with test standard sample.

Organic carbon (OC) and elemental carbon (EC) in each sample were determined with the use of a DRI Model 2001 Thermal/Optical Carbon Analyzer (Atmoslytic Inc., Calabasas, CA, USA). The thermal/optical reflectance (TOR) method and IMPROVE_A protocol were used for analysis. A punch of a quartz filter sample was heated at specific temperatures to obtain data for four OC fractions and three EC fractions. Total OC was calculated by summing all OC fractions and the pyrolyzed carbon (OP) produced. Total EC was calculated by summing all EC fractions minus the OP. Detailed methods and quality assurance/quality control processes were described in Cao et al., (2003). Primary organic carbon (POC) was estimated by using the minimum R-squared (MRS) method, which is based on using eBC as a tracer (Text S1). The method uses the minimum R^2 between OC and eBC to indicate where the ratio for which secondary OC and eBC are independent. A detailed description of the MRS method can be found in Wu et al., (2016).

Data for NO_x , wind speed, and direction at 12 ground monitoring sites were downloaded from http://sthjt.shaanxi.gov.cn/hx_html/zdjkqy/index.html. The wind data at 100 meters (m) above the ground and the planetary boundary layer height were downloaded from <https://rda.ucar.edu/datasets/ds633.0>. The data used for the Hybrid Single-Particle Lagrangian Integrated Trajectory (HYSPLIT) model was downloaded from Global Data Assimilation System and it had a resolution of $1^\circ \times 1^\circ$ (GDAS, <https://www.ready.noaa.gov/gdas1.php>). The data and main parameters used in trajectory model are listed in Table S2.”

2.3 Optical source apportionment

The positive matrix factorization (PMF) model that was used for the optical source apportionment in this study. PMF solves chemical mass balance by decomposing the observational data into different source profiles and contribution matrices as follows:

$$X_{ij} = \sum_{k=1}^p g_{ik} f_{kj} + e_{ij} \quad (1)$$

where X_{ij} denotes the input data matrix; p is the number of sources selected in the model; g_{ik} denotes the contribution of the k^{th} factor to the i^{th} input data; f_{kj} represents the k^{th} factor's profile of the j^{th} species; and e_{ij} represents the residual. Both g_{ik} and f_{kj} are non-negative. The uncertainties of each species and $b_{\text{abs}}(\lambda)$ were calculated by the equation recommended in EPA PMF5.0 user guideline (Norris et al, 2014) as follows:

$$Unc = \sqrt{(\text{error fraction} \times \text{concentration}(\text{or light absorption coefficient}))^2 + (0.5 \times MDL)^2} \quad (2)$$

$$Unc = \frac{5}{6} \times MDL \quad (3)$$

where MDL is the minimum detection limit of the method. When the concentration of a species was higher than the MDL then equation (2) was used otherwise equation (3) was used. In equation (2), for calculating the uncertainty of a chemical species, the error fraction was multiplied the concentration of the species. For calculating the uncertainty of optical data, the error fractions were multiplied by the light absorption coefficients.

Chemical species data (EC, POC, K^+ , Mg, Al, Si, S, Cl, Ca, V, Mn, Fe, Ni, Cu, As, Se, Br, Sr, Pb, Ga and Zn) and the primary absorption coefficients (Pabs) data at $\lambda=370\text{nm}, 470\text{nm}, 520\text{nm}, 660\text{nm}$, and 880nm were used for PMF analysis. The error fraction of offline measured data was the difference between multiple measurements of the same sample. The error fraction used for optical data was 10% based on Rajesh and Ramachandran (2018). PMF solves the equation (1) by minimizing the Q value, which is the sum of the normalized residuals' squares, as follows,

$$Q = \sum_{i=1}^n \sum_{j=0}^n \left[\frac{e_{ij}}{u_{ij}} \right]^2 \quad (4)$$

where u_{ij} represents the uncertainties of each X_{ij} and $Q_{\text{true}}/Q_{\text{exp}}$ was used as the indicators for the factor number determination.

2.4 eBC source apportionment

The quantities of eBC generated from biomass burning versus fossil fuel combustion were deconvolved by an aethalometer model which uses Beer-Lambert's Law to write the absorption coefficients equations, wavelengths and absorption Ångström exponents (AAEs) for the two different BC emission sources (Sandradewi et al., 2008). This approach is widely used for separating BC from two different sources based on optical data (Rajesh et al., 2018; Kant et al., 2019; Panicker et al., 2010). However, the traditional aethalometer model could be affected by the light absorbing substances at lower wavelengths such as dust and secondary formation particles. An improvement to the traditional aethalometer model was made, by explicitly considering the interference of the b_{abs} at a lower wavelength (370nm) caused by dust and secondary OC. Thus, the calculation of the absorption and source apportionment was based on the following equations (Wang et al., 2020):

$$\frac{b_{\text{abs}}(370)_{\text{fossil}}}{b_{\text{abs}}(880)_{\text{fossil}}} = \left(\frac{370}{880} \right)^{-AAE_{\text{fossil}}} \quad (5)$$

$$\frac{b_{\text{abs}}(370)_{\text{biomass}}}{b_{\text{abs}}(880)_{\text{biomass}}} = \left(\frac{370}{880} \right)^{-AAE_{\text{biomass}}} \quad (6)$$

$$b_{\text{abs}}(880) = b_{\text{abs}}(880)_{\text{fossil}} + b_{\text{abs}}(880)_{\text{biomass}} \quad (7)$$

$$b_{\text{abs}}(370) = b_{\text{abs}}(370)_{\text{fossil}} + b_{\text{abs}}(370)_{\text{biomass}} + b_{\text{abs}}(370)_{\text{secondary}} + b_{\text{abs}}(370)_{\text{dust}} \quad (8)$$

$$eBC_{\text{fossil}} = \frac{b_{\text{abs}}(880)_{\text{fossil}}}{MAC_{BC}(880)_{\text{fossil}}} \quad (9)$$

$$eBC_{\text{biomass}} = \frac{b_{\text{abs}}(880)_{\text{biomass}}}{MAC_{BC}(880)_{\text{biomass}}} \quad (10)$$

where AAE_{fossil} and AAE_{biomass} are the AAEs for fossil fuel combustion and biomass burning. These were derived from the optical source apportionment by using PMF as discussed in section 3.1. Further, $b_{\text{abs}}(370)$ and $b_{\text{abs}}(880)$ are the total b_{abs} measured by the AE33 at the wavelengths of 370 nm and 880 nm respectively; $b_{\text{abs}}(370)_{\text{fossil}}$ and $b_{\text{abs}}(880)_{\text{fossil}}$ are the b_{abs} caused by emissions from fossil fuel combustion at those two wavelengths; $b_{\text{abs}}(370)_{\text{biomass}}$ and $b_{\text{abs}}(880)_{\text{biomass}}$ are the b_{abs} caused by emissions from biomass burning at those two wavelengths; $b_{\text{abs}}(370)_{\text{dust}}$ refers to the b_{abs} contributed by mineral dust at the wavelength of 370 nm, which was derived from the result of optical source apportionment; $b_{\text{abs}}(370)_{\text{secondary}}$ refers to the b_{abs} caused by the secondary aerosols at the wavelength of 370 nm, which was calculated by the minimum R -squared approach with eBC as a tracer (Text S1, Wang et al., 2019); eBC_{fossil} and eBC_{biomass} are the eBCs from fossil fuel combustion and biomass burning; and $MAC_{BC}(880)_{\text{fossil}}$ and $MAC_{BC}(880)_{\text{biomass}}$ are the mass absorption cross-sections of eBC_{fossil} and the mass absorption cross-section of eBC_{biomass} at the wavelength of 880 nm respectively, which were based on the PMF results for the optical source apportionments.

2.5 Indicators for the different scales of motion

The mathematical definitions of airflow condition proposed by Allwine and Whiteman (1994) were used in this study. The definitions quantify the flow features integrally at individual stations. Three variables were quantified, namely the actual wind run distance (S) which is the scalar displacement of the wind in 24 h (i.e.

the accumulated distance of the wind), the resultant transport distance (L) which is the vector displacement of the wind in 24 h (i.e. the straight line from the starting point to the end point), and the recirculation factor (R) is based on the ratio of L and S which indicates the frequency of the wind veering in 24 h. The influences of different scales of atmospheric motions were assessed based on the method proposed by Levy et al., (2010), and for this, we used wind data at 100 m above the sampling site and the wind data from 12 monitoring stations at ground level (~15m) to indicate the different scales of motions. The winds at the surface monitoring stations were expected to be more sensitive to local-scale turbulence and convection than the winds at 100 m. With less influence from the surface forces, the indicators at 100 m would be more sensitive to larger scales of motion. The equations used as follows:

$$L_{n\tau/bj} = T \left[\left(\sum_{j=i}^{i-\tau+1} u_i \right)^2 + \left(\sum_{j=i}^{i-\tau+1} v_i \right)^2 \right]^{1/2} \quad (11)$$

$$S_{n\tau/bj} = \sum_{j=i}^{i-\tau+1} (u_j^2 + v_j^2)^{1/2} \quad (12)$$

$$R_{n\tau/bj} = 1 - \frac{L_{i\tau}}{S_{i\tau}} \quad (13)$$

where T is the interval of the data (i.e., 60 min), i is the i^{th} the ending time step data, τ is the integration time period of the wind run (24 h), $i-\tau+1$ represents the data at the start time, and n is the number of monitoring stations (a total of 12 in this study). The quantities u and v are the wind vectors. Using the wind data from the 12 monitoring stations covering Baoji, the L and S values at the 12 different sites at ground level were calculated. $L_{n\tau}$ and $S_{n\tau}$ represent the resultant transport distance and the actual wind run distance at the n^{th} ($n = 1$ to 12) monitoring station at ground level; $R_{n\tau}$ is the recirculation factor at the n^{th} monitoring station which is calculated based on $L_{n\tau}$; and $S_{n\tau}$; L_{bj} , and S_{bj} are the resultant transport distance and the actual wind run distance at 100 m height above the ground. These represent the flow characteristics in higher atmosphere at the study site, and they were calculated by using the wind data at 100 m height. The recirculation factor (R_{bj}) was calculated for a height of 100 m.

As explained in Levy et al., (2010), if local-scale motions are strong and regional-scale motions are weak, the variations in winds at each station would not be likely to be uniform due to differences in local factors, and that would result in relatively large standard deviations (R_{std}) for $R_{n\tau}$. By contrast, if the local-scale motions are weak and the regional-scale motion is strong, the wind direction would be likely to be more uniform over a large area, and the R_{bj} and the R_{std} should be relatively smaller.

2.6 Self-organizing map

A self-organizing map (SOM) developed by Kohonen (1990) is a type of artificial neural network that is widely used for categorizing high-dimensional data into a few major features (Stauffer et al., 2016 and Pearce et al., 2014). In particular, this approach is widely used for categorizing different meteorological patterns (Liao et al., 2020; Han et al., 2020; Jiang et al., 2017). Unlike traditional dimension reduction methods (e.g., principal component analysis), SOM projects high-dimensional input data by non-linear projection into user-designed lower-dimensions, which are typically two-dimensional arrays of nodes (Hewitson and Crane, 2006). The performance of SOM in classifying climatological data has been shown to be robust (Reusch et al., 2005). Competitive learning algorithms are used to train SOM, and the architecture of SOM consists of two layers; one is called the input layer and it contains the high dimensional input data. The other layer is the output layer in which the node number is the output cluster number. The working principle of SOM is to convert high dimensional data with complex correlations into lower dimensions via geometrical relationships (Ramachandran et al., 2019). After the initial random weights are generated, the input data are compared with each weight, and the best match is defined as winning. The winning node and the neighboring nodes close to the winning node will learn from the same inputs and the associated weights are updated. After multiple iterations, the network settles into stable zones of features and the weights.

More detailed working principles of SOM can be found Kangas and Kohonen, (1996) and Kohonen et al., (1996).

Comparison between the input data and each weight is made by applying Euclidean distances, the best match is defined by the following equation:

$$\|x - m_c\| = \min\{\|x - m_i\|\} \quad (14)$$

where x is the input data, m_c is the best matched weight, m_i is the weights connected with the i^{th} node.

The weights are updated by following equation:

$$m_i(t + 1) = m_i(t) + h_{ci}(t)[x(t) - m_i(t)] \quad (15)$$

where the $m_i(t + 1)$ is the i^{th} weight at $t+1$ time, $m_i(t)$ is the i^{th} weight at t time, the $h_{ci}(t)$ is the neighborhood kernel defined over the lattice points at t time, and c is the winning node location.

SOM was used to categorize the daily atmospheric motions during the study period and to explore the influences of different scales of motion on source-specific eBC. Hourly averages of three sets of data (R_{std} , L_{bj} , and S_{bj}) were input into SOM. Determining the size of the output map is crucial for SOM (Chang et al 2020 and Liu et al., 2021). To reduce the subjectivity, the K-means cluster method was used for the decision-making regarding size. The similarity of each item of the input data relative to the node was measured using Euclidean distance. The iteration number was set to 2000. For each input data item, the node closest to it would “win out”. The reference vectors of the winning node and their neighborhood nodes were updated and adjusted towards the data. The “Kohonen” package in R language (Wehrens and Kruisselbrink, 2019) was used to develop the SOM model in this study.

2.7 Estimations of direct radiative effects and heating rate

The Santa Barbara DISORT Atmospheric Radiative Transfer (SBDART) model was used to estimate the direct radiative effects (DRE) induced by source-specific eBC. The model has been used in many studies to calculate the DRE caused by aerosols and BC (Pathak et al., 2010; Rajesh et al., 2018; Zhao et al., 2019). SBDART calculated DRE based on several well-tested physical models. Details regarding the model were presented in Ricchiazzi et al., (1998). The important input data included aerosol parameters, including aerosol optical depth (AOD), single scattering albedo (SSA), asymmetric factor (AF) and extinction efficiency, surface albedo, and atmospheric profile.

The aerosol parameters used in this study were derived by the Optical Property of Aerosol and Cloud (OPAC) model (Hess et al., 1998) based on the number concentrations of aerosol components. As the study was conducted in an urban region, the urban aerosol profile was used in OPAC, and it included soot (eBC), water-soluble matter (WS), and water-insoluble matter (WIS). The number concentrations of soot were derived from the mass concentrations of eBC with the default ratio ($5.99\text{E-}5 \mu\text{g m}^{-3}/ \text{particle.cm}^{-3}$) in OPAC. The number concentrations of WS and WIS were adjusted until the modeled SSA and b_{abs} at 500nm in OPAC were close ($\pm 5\%$, see Figure S4) to those values calculated with data from the nephelometer and AE33 ($b_{\text{ext}}(520) = b_{\text{scat}}(525) + b_{\text{abs}}(520)$, $\text{SSA} = b_{\text{scat}}(525)/b_{\text{ext}}(520)$). The DRE of source-specific eBC at the top of atmosphere (TOA) and surface atmosphere (SUF) were calculated from the difference between the DREs with or without the number concentrations of the source-specific eBC under clear-sky conditions.

$$DRE_{eBC} = (F \downarrow - F \uparrow)_{\text{with } eBC} - (F \downarrow - F \uparrow)_{\text{without } eBC} \quad (16)$$

$$DRE_{eBC,ATM} = DRE_{eBC,TOA} - DRE_{eBC,SUF} \quad (17)$$

where DRE_{eBC} is the DRE of source-specific eBC, $F\downarrow$ and $F\uparrow$ are the downward and upward flux, $DRE_{eBC,ATM}$ is the DRE of the source-specific eBC for the atmospheric column, that is, the DRE at the top of the atmosphere ($DRE_{eBC,TOA}$) minus that at the surface ($DRE_{eBC,SUF}$)”

“Text S1. Minimum R - squared method

The minimum R squared method developed by Wu et al., (2016) was used to separate secondary organic carbon (SOC) from the primary organic carbon (POC). The assumption behind this method is the organic carbon (OC) from non-combustion source is negligible. As explained by Wang et al., (2019), the major non-combustion source is biogenic which is mainly exists in coarse mode. Thus, the non-combustion organic carbon is considered negligible in this study. Therefore, SOC and POC can be separated by using following equations. For each date set, the ratios of OC to eBC and SOC and the R^2 between eBC and SOC can be calculated. SOC and eBC are considered independent, so the $(OC/eBC)_{pri}$ should be the value obtained when the R^2 between eBC and SOC is minimum.

$$POC = (OC/EC)_{pri} \times EC \quad (S1)$$

$$SOC = OC_{total} - (OC/EC)_{pri} \times EC \quad (S2)$$

where EC in this study is eBC. The $(OC/EC)_{pri}$ is the ratio in freshly emitted OC and EC from combustion sources.

The light absorption at shorter wavelengths (<660nm) is not only from primary light absorbing substances but also from the secondary organic carbon (Wang et al., 2019). The assumption for this method is that the light absorption caused by non-combustion sources is negligible. As mentioned above, most of the biogenic BrC is in coarse mode. Another common light absorbing substance is the Fe_2O_3 in the dust, but the impact of that should be limited because the absorption from Fe_2O_3 in the dust has been reported to be much smaller than that from BC (Ramachandran and Kedia, 2010). Thus, to separate the secondary light absorption ($b_{abs}(\lambda)_{secondary}$) from the primary light absorption ($b_{abs}(\lambda)_{primary}$), a BC-tracer method coupled with a minimum R-squared method was used. The equations used for the calculation are follows:

$$b_{abs}(\lambda)_{secondary} = b_{abs}(\lambda) - \left(\frac{b_{abs}(\lambda)}{BC}\right)_{pri} \times BC \quad (S3)$$

$$b_{abs}(\lambda)_{primary} = b_{abs}(\lambda) - b_{abs}(\lambda)_{secondary} \quad (S4)$$

Where $b_{abs}(\lambda)$ is the light absorption at different wavelengths ($\lambda=370nm, 470nm, 520nm, 590nm, 660nm$) measured by AE33, BC is the eBC measured by AE33 at a wavelength of 880nm. The $\left(\frac{b_{abs}(\lambda)}{BC}\right)_{pri}$ is the ratio of the primary light absorption to the BC mas concentration from combustion sources.

Text S2. Cluster analysis of air-mass trajectories

Back trajectories were calculated by using Hybrid Single-Particle Lagrangian Integrated Trajectory (HYSPLIT) model (Draxler and Hess, 1998) developed by the Air Resource Lab (ARL) of the National Oceanic and Atmospheric Administration (NOAA). The model can predict the position of air mass by using mean wind. The back-in-time positions are calculated by reversing the advection equation (Draxler and Hess, 1997). The calculation requires the mean wind, for calculating trajectories, only advection is considered (Stein et al., 2015). The basic equations for trajectory calculation in HYSPLIT are as follows:

$$P'(t + \Delta t) = P(t) + V(P, t) \times \Delta t \quad (S5)$$

$$P(t + \Delta t) = P(t) + 0.5 \times [V(P, t) + V(P', t + \Delta t)] \times \Delta t \quad (S6)$$

Where $P(t)$ is the initial position, $P'(t + \Delta t)$ is the first guess position, V is the average velocity, t is the time, Δt is the time step.

A large number of 24 h trajectories (793) that were retrieved for the study period showed diverse pathways, so in order to find out the representative pathways for those trajectories, a cluster analysis based on an angle-based distance statistics method was conducted. Compared with Euclidean distance, angle-based distance statistics method focuses on the direction of air mass instead of the speed. The angle-based distance statistics method is defined by following equations (Sirois and Bottenheim, 1995):

$$d_{12} = \frac{1}{2} \sum_{i=1}^n \cos^{-1} \left(0.5 \times \frac{A_i + B_i - C_i}{\sqrt{A_i B_i}} \right) \quad (S7)$$

$$A_i = (X_1(i) - X_0)^2 + (Y_1(i) - Y_0)^2 \quad (S8)$$

$$B_i = (X_2(i) - X_0)^2 + (Y_2(i) - Y_0)^2 \quad (S9)$$

$$C_i = (X_2(i) - X_1(i))^2 + (Y_2(i) - Y_1(i))^2 \quad (S10)$$

Where d_{12} is the average angle between the two backward trajectories, varying between 0 and π ; X_0 and Y_0 are the position of the receptor site; and X_1 (Y_1) and X_2 (Y_2) are the backward trajectories 1 and 2, respectively. In this study, three clusters were chosen as representative of the backward trajectory clusters based on the total spatial variance (TSV) value. The simulation was conducted using the GIS-based TrajStat software (Wang et al., 2009).”

Specific comments

Abstract:

“Black carbon (BC) has a strong light absorption ability and is known as the second strongest light-absorbing substance in the atmosphere after CO₂” This is debatable.

Response: We have corrected the sentence into “Black carbon (BC) is one of the most important short lived climate forcers, and atmospheric motions play an important role in determining its mass concentrations of pollutants.”

In the first paragraph in the introduction part, we also revise the relevant sentence into:

“Black carbon (BC) is produced by the incomplete combustion of biomass and fossil fuels. The BC aerosol has a strong light absorption capacity and can cause heating of the atmosphere. In fact, BC is widely recognized as one of the most important short-lived climate forcers (IPCC, 2021).”

What does model refer to in “aethalometer model”?

Response: The model refers to the calculation model based on Beer–Lambert’s Law. The model contains a few equations relating the absorption coefficients (b_{abs}), the wavelengths, and the absorption exponents for conditions of two BC emission sources (Sandradewi et. al., 2008). In this study the two sources were fossil

combustion and biomass burning. We have revised the method section 2.4 to provide a better description and reference. The revised version was provided in response above.

Reference:

Sandradewi, J., Prévôt, A. S. H., Weingartner, E., Schmidhauser, R., Gysel, M., and Baltensperger, U.: A study of wood burning and traffic aerosols in an Alpine valley using a multi-wavelength Aethalometer, *Atmos. Environ.*, 42, 101-112, <https://doi.org/10.1016/j.atmosenv.2007.09.034>, 2008.

“chemical data and optical data” what kind of data?

Response: The chemical data includes EC, POC, K⁺, Mg, Al, Si, S, Cl, Ca, V, Mn, Fe, Ni, Cu, As, Se, Br, Sr, Pb, Ga, and Zn. The optical data refers to primary absorption coefficient ($b_{\text{abs}}(\lambda)$) at six wavelengths ($\lambda = 370, 470, 520, 590, 660, \text{ and } 880 \text{ nm}$). To make this clear, we have revised the relevant sentence into

“Equivalent BC (eBC) source apportionment was based on an aethalometer model with the site-dependent absorption Ångström exponents (AAEs) and the mass absorption cross-sections (MACs) retrieved using a positive matrix factorization (PMF) model based on observed chemical components (i.e. EC, POC, K⁺, Mg, Al, Si, S, Cl, Ca, V, Mn, Fe, Ni, Cu, As, Se, Br, Sr, Pb, Ga, and Zn) and primary absorption coefficients at selected wavelengths from $\lambda = 370$ to 880 nm .”

“The derived AAEs” over what wavelength range?

Response: The AAEs were obtained by the power fit of b_{abs} from 370nm, 470nm, 520nm, 660nm and 880nm. The fitting is shown in figure R3. We also added this figure into supplement material and revised the relevant sentence shown below:

“The derived AAEs from 370 to 880nm were 1.07 for diesel vehicular emissions, 2.13 for biomass burning, 1.74 for coal combustion, and 1.78 for mineral dust. The mean values for $\text{eBC}_{\text{fossil}}$ and $\text{eBC}_{\text{biomass}}$ were $2.46 \mu\text{g m}^{-3}$ and $1.17 \mu\text{g m}^{-3}$ respectively.”

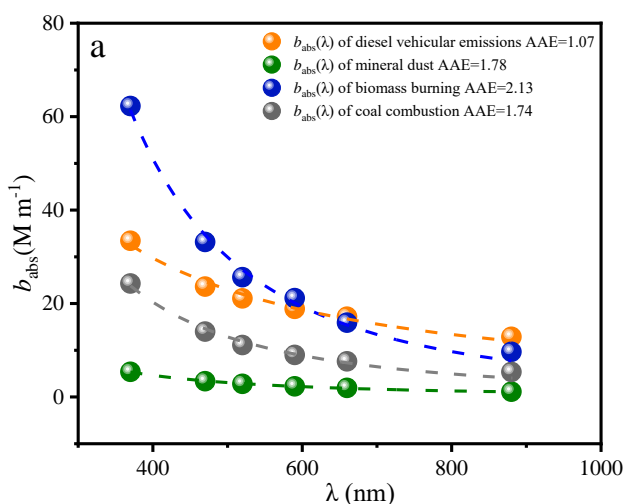


Figure R3 Light absorption ($b_{\text{abs}}(\lambda)$) for diesel vehicular emissions, biomass burning, coal combustion, and mineral dust. The dashed lines are the power law fits.

“four featured atmospheric motions categories” what the four categories are remains a mystery until later, please provide a brief description here because the abstract should be self-contained.

Response: Thanks for the suggestion, we have revised this sentence to add more information on the four categories as follows:

“Wind run distances and the vector displacements of the wind in 24 h were used to construct a self-organizing map, from which four atmospheric motions categories were identified (local-scale dominant, local-scale strong and regional-scale weak, local-scale weak and regional-scale strong and regional-scale dominant).”

“The trajectory clusters” what trajectories? How were those determined?

Response: The trajectories in this study reconstruct the path the air mass moved through in time and space. The back trajectories were calculated by using Hybrid Single-Particle Lagrangian Integrated Trajectory (HYSPLIT) model (Draxler and Hess, 1998). The model can predict the position of air mass by using the mean winds. The backwards-in-time position is calculated by reversing the advection equation (Draxler and Hess, 1997). The calculation needs the mean wind, for running trajectories, and only advection is considered (Stein et al., 2015). The basic equations for trajectory calculation in HYSPLIT are as followings:

$$P'(t + \Delta t) = P(t) + V(P, t) \times \Delta t \quad (\text{R1})$$

$$P(t + \Delta t) = P(t) + 0.5 \times [V(P, t) + V(P', t + \Delta t)] \times \Delta t \quad (\text{R2})$$

Where $P(t)$ is the initial position, $P'(t + \Delta t)$ is the first guess position, V is the average velocity, t is the time, Δt is the time step.

To this clear, we have revised the sentence into “Cluster analysis for the back trajectories of air mass calculated by Hybrid Single-Particle Lagrangian Integrated Trajectory model at the study site indicated that the directions of air flow can have different impacts for different scales of motion.” And added the method description above into the supplementary material (Text S2) and provided a Table (Table S2) to show the input data, main parameters used in this study as follow:

Table R3 Data and parameters used in HYSPLIT model

| Items | Data/parameters |
|------------------------|--------------------------------------------------------------------|
| Model | HYSPLIT |
| Meteorological data | GDAS data, $1^\circ \times 1^\circ$, 23 vertical levels, 3 hourly |
| Backward period | 24h |
| Footprint level | 100 m above the ground |
| Receptor site location | $34^\circ 21' 16.8''\text{N}$, $107^\circ 12' 59.6''\text{E}$ |

Reference:

Stein, A., Draxler, R., Rolph, G., Stunder, B., Cohen, M., and Ngan, F.,: NOAA’S HYSPLIT Atmospheric Transport and Dispersion Modeling System, Bull. Amer. Meteor. Soc., 96, 2059-2077, <https://doi.org/10.1175/BAMS-D-14-00110.1>, 2015.

Draxler, R., and Hess, G.: An overview of the HYSPLIT_4 modelling system for trajectories, Aust. Meteorol. Mag., 47, 1998.

Lines 30-31: I don’t understand the sentence “This study revealed the disproportional change between BC mass concentration and its DRE.”

Response: We apologize for the confusing expression, and we would like to provide a further explanation and have revised the sentence to make it clear.

If the light absorbing ability is independent of the patterns of the motion (which indicates a possible path and distance the BC moved in atmosphere), the value of DRE per unit mass of BC should be the same for all cases. However, in this study, both DREs and the mass concentrations of eBC_{fossil} and eBC_{biomass} changed. If we normalize DRE by dividing the mass concentration of eBC, we can see that a unit of eBC of both types associated with higher DRE under local scale weak and regional scale strong motion (LWRS) and regional scale dominance motion (RD) as shown in Table R4. If we take local scale dominance (LD) as a reference case to calculate the difference between averaged BC mass concentration (or averaged DRE) under LD and other cases (LSTW, LWRS and RD). It is apparent that the BC mass concentrations decreased more than DRE did (Table R5).

To avoid confusion, we revised the sentence into “The finding that the DRE efficiency of BC increased during the regional transport suggested significant consequences in regions downwind of pollution sources and emphasizes the importance of regionally transported BC for potential climatic effects.” And “Similar to the mass concentrations, the DREs of the two types of eBC were both lower when the regional scale of motions were greater than the local ones. However, the changes in mass concentrations and DREs were not proportionate because the regional-scale of motions carried the fresh BC away from the local site but brought the aged BCs to the site from the upwind regions. As a result, the DRE efficiency of eBC was ~1.5 times higher when the regional scale of motion was stronger.”

Table R4. Direct radiative forcing efficiencies for equivalent black carbon (eBC) from fossil fuel combustion (eBC_{fossil}) and the eBC from biomass burning

| Atmospheric motion category | DRE _{eBC_{fossil}, ATM} efficiency ^a ((W m ⁻²)/(μg m ⁻³)) | DRE _{eBC_{biomass}, ATM} efficiency ^a ((W m ⁻²)/(μg m ⁻³)) |
|---------------------------------------------------|------------------------------------------------------------------------------------------------------------------|-------------------------------------------------------------------------------------------------------------------|
| Local scale dominance (LD) | 10.2 ± 4.2 | 10.3 ± 4.4 |
| Local scale strong and regional scale weak (LSRW) | 10.6 ± 5.7 | 10.2 ± 5.8 |
| Local scale weak and regional scale strong (LWRS) | 13.5 ± 6.7 | 14.7 ± 8.1 |
| Regional scale dominance (RD) | 15.6 ± 8.9 | 15.5 ± 8.4 |

a: Mean ± Std

Table R5 The change of mass concentration of different eBCs and their DREs

| Atmospheric motion category | Change of mass concentration of eBC _{fossil} | Change of mass concentration of eBC _{biomass} | Change of DRE _{eBCfossil, ATM} | Change of DRE _{eBCbiomass, ATM} |
|-----------------------------|-------------------------------------------------------|--------------------------------------------------------|-----------------------------------------|------------------------------------------|
| LD | - | - | - | - |
| LSRW | 9.4% | 30.3% | 5.7% | -2.9% |
| LWRS | 30.2% | 43.4% | 29.3% | 23.1% |
| RS | 45.1% | 38.8% | 34.6% | 29.0% |

Line 32: “It highlights...” what does “it” refer to? In general, this closing sentence reads awkward, and I would suggest rewording it.

Response: Thanks for pointing this out, we have revised the sentence as follows:

“The finding that the DRE efficiency of BC increased during the regional transport suggested significant consequences in regions downwind of pollution sources and emphasizes the importance of regionally transported BC for potential climatic effects.”

Introduction:

Light absorbing or agent with positive radiative forcing? The two whings are linked but not the same.

Response: We agree with reviewer. Based on IPCC (2021) and most studies on BC (Zhao, et al., 2019; Panicker et al., 2010; Rajesh and Ramachandran, 2018, Valenzuela et al., 2017) direct radiative forcing, BC generally is considered to be a short life climate forcer which can warm the climate, however for other types of aerosols, their scattering ability is higher than its absorbing ability which more likely leads to negative forcings.

We have revised the sentence into:

“Black carbon (BC) is produced by the incomplete combustion of biomass and fossil fuels. The BC aerosol has a strong light absorption capacity and can cause heating of the atmosphere. In fact, BC is widely recognized as one of the most important short-lived climate forcings (IPCC, 2021).”

Reference:

IPCC: Climate Change 2021: The Physical Science Basis. Contribution of Working Group I to the Sixth Assessment Report of the Intergovernmental Panel on Climate Change [Masson-Delmotte, V., P. Zhai, A. Pirani, S.L. Connors, C. Péan, S. Berger, N. Caud, Y. Chen, L. Goldfarb, M.I. Gomis, M. (eds)], <https://reliefweb.int/report/world/climate-change-2021-physical-science-basis>, 2021

Zhao, S. P., Yu, Y., Yin, D., Yu, Z., Dong, L. X., Mao, Z., He, J. J., Yang, J., Li, P., and Qin, D. H.: Concentrations, optical and radiative properties of carbonaceous aerosols over urban Lanzhou, a typical valley city: Results from in-situ observations and numerical model, *Atmos. Environ.*, 213, 470–484, <https://doi.org/10.1016/j.atmosenv.2019.06.046>, 2019.

Panicker, A. S., Pandithurai, G., Safai, P. D., Dipu, S., and Lee, D.-I.: On the contribution of black carbon to the composite aerosol radiative forcing over an urban environment, *Atmos. Environ.*, 44, 3066-3070,

10.1016/j.atmosenv.2010.04.047, 2010.

Rajesh, T. A., and Ramachandran, S.: Black carbon aerosols over urban and high altitude remote regions: Characteristics and radiative implications, *Atmos. Environ.*, 194, 110-122, <https://doi.org/10.1016/j.atmosenv.2018.09.023>, 2018.

Valenzuela, A., Arola, A., Anon, M., Quirantes, A., Alados-Arboledas, L.: Black carbon radiative forcing derived from AERONET measurements and models over an urban location in the southeastern Iberian Peninsula, *Atmospheric Research*, 191, 44–56, <http://dx.doi.org/10.1016/j.atmosres.2017.03.007>, 2017.

Line 55: remove “at” before “to”

Response: Thanks for the correction, we have revised this sentence. Now the sentence is:

“The concentrations of BC are controlled by local emissions and regional transport, but meteorological conditions also are important because they affect both transport and removal. Normally, local emissions in urban areas are predictable to some degree because those emission sources are mainly anthropogenic and the concentrations of pollutants follow the diurnal patterns driven by anthropogenic activities.”

Line 57: multiply -> multiple

Response: We apologize for the misspelling. It has been corrected in the revised version.

“By contrast, meteorological conditions and regional transport are governed by multiple scales of motion which result in distinct meteorological impacts on ambient pollutant levels (Levy et al., 2010, Dutton, 1976).”

Line 62: Why the aerosol concentration controls the local scale motion?

Response: Horizontal temperature variations can give rise to pressure differences, which can result in atmospheric motions (Oke, 1988). The aerosol concentrations and types (i.e. dominance of scattering aerosol or absorbing aerosol) can impact on the temperature, and changes in cloud microphysical properties also can impact the temperature (IPCC, 2021). Thus, difference of aerosol mass concentrations between locations could lead to atmospheric motions.

Reference:

Oke, T., *Boundary Layer Climates*, 2nd edition, Taylor & Francis e-Library, 2002.

IPCC: *Climate Change 2021: The Physical Science Basis. Contribution of Working Group I to the Sixth Assessment Report of the Intergovernmental Panel on Climate Change* [Masson-Delmotte, V., P. Zhai, A. Pirani, S.L. Connors, C. Péan, S. Berger, N. Caud, Y. Chen, L. Goldfarb, M.I. Gomis, M. (eds)], <https://reliefweb.int/report/world/climate-change-2021-physical-science-basis>, 2021

Line 64: diffuse -> disperse?

Response: Thanks for the comment, we have corrected this.

“Larger scale of motions are associated with a mesoscale or synoptic scale weather systems, which on the one hand can transport pollutants but on the other can disperse them (Kalthoff et al., 2000; Zhang et al., 2012).”

Line 65: “decides” seems more to belong to an intelligent entity. Maybe “determines”

Response: Thanks for explaining the difference between the two words. We have changed the “decides” into

“determines”.

“The relationships between atmospheric motions and pollutant concentrations are complex. Atmospheric motions determine where and how extensive the pollution impacts are, but of course the rates of pollutant emissions, especially local ones, are important, too (Dutton, 1976).”

Line 72: “river valley city” comes a bit out of the blue here, it might be good to provide a sentence with some background, like the general location, etc., even if that’s then discussed in detail in the method section. Is the city specifically Baoji?

Response: We agree that providing some background information would make it is more coherent, so we rewrote this part as follows:

“Topography also plays an important role in air pollution (Zhao et al., 2015). River-valley topography is complicated, and it can have a considerable influence on air pollution and synoptic patterns of flow (Green et al., 2016; Carvalho et al., 2006). The pollution levels at cities in river-valleys are not only influenced by general atmospheric dynamics but also strongly impacted by the local-scale of dynamics (Brulfert et al., 2006). Surface albedo and surface roughness are affected by the complex topography of river-valley regions, and those physical factors can affect circulation causing changes in pollutant mass concentrations (Wei et al., 2020). Mountains also significantly affect pollution, and once pollutants are generated or transported into the river-valley regions, their dispersal can be impeded by the blocking effect of the mountains. Instead of being dispersed, they can be carried by the airflows over the mountains to converge at the bottom of the valley and increase the pollutants along the river (Zhao et al., 2015). In this way, pollutants can accumulate in valleys and spread throughout the area, thereby aggravating pollution. In addition, temperature inversions commonly form in river-valleys during the winter, and that, too, can aggravate pollution problems (Glojek et al., 2022 and Bei et al., 2016).”

The river valley city we referred here is not just baoji. This topography (river-valley) has been found impact on air pollution and synoptic patterns in other countries as well (Brulfert et al., 2006, Green et al., 2016, Glojek et al., 2022).

Reference

Glojek, K., Močnik, G., Alas, H., Cuesta-Mosquera, A., Drinovec, L., Gregorič, A., Ogrin, M., Ježek, I., Müller, T., Rigler, M., Remškar, M., Pinxteren, D., Herrmann, H., Ristorini, M., Merkel, M., Markelj, M., Wiedensohler, A.: The impact of temperature inversions on black carbon and particle mass concentrations in a mountainous area, *Atmos. Chem. Phys.*, 22, 5577–5601, <https://doi.org/10.5194/acp-22-5577-2022>, 2022.

Brulfert, G., Chemel, C., Chaxel, E., Chollet, J., Jouve, B., and Villard, H.: Assessment of 2010 air quality in two Alpine valleys from modelling: Weather type and emission scenarios, *Atmos. Environ.*, 40, 7893–7907, <https://doi.org/10.1016/j.atmosenv.2006.07.021>, 2006.

Green, M., Chow, J., and Watson, G.: Effects of Snow Cover and Atmospheric Stability on Winter PM_{2.5} Concentrations in Western U.S. Valleys, *Journal of Applied Meteorology and Climatology.*, 54, <https://doi.org/doi:10.1175/JAMC-D-14-0191.1>, 2016.

Line 75: why the albedo makes the solar radiation uneven? Do they mean the reflected radiation? In general, I find this sentence awkward and unclear.

Response: Surface albedo is the ratio of up-welling to down-welling short wave radiative flux at the surface ($Albedo = \frac{Reflected\ radiation}{Incident\ radiation}$). Surface albedo is one of the most important parameters for determining radiative

forcing and it impacts on climatic processes. The spatial and temporal distribution of surface properties captured by albedo reflect a variety of natural and human influences on the surface that are of importance in terms of radiative balance. Surface albedos vary with the type of surface; for example the albedo for the ocean is much lower than that of land (Satheesh et al., 2006), the surface albedo of vegetated lands is also different from that of urban areas. Studies found that lower surface albedos, compared with higher ones, result in more positive radiative forcing at the top of the atmosphere (Nari et al., 2013 and reference therein).

We have rewritten that sentence from line 75 as following and hope it now reads clear and understandable.

“Surface albedo and surface roughness are affected by the complex topography of river-valley regions, and those physical factors can affect circulation causing changes in pollutant mass concentrations (Wei et al., 2020).”

The sentence starting on line 77 is also awkward and should be reworded.

Response: We have revised this sentence, now it reads like:

“Mountains also significantly affect pollution, and once pollutants are generated or transported into the river-valley regions, their dispersal can be impeded by the blocking effect of the mountains. Instead of being dispersed, they can be carried by the airflows over the mountains to converge at the bottom of the valley and increase the pollutants along the river (Zhao et al., 2015).”

Line 80: eBC appears here without having been defined as equivalent BC. It has been defined only later, but it should be defined at its first appearance.

Response: Thanks for pointing this out. We have added the definition of eBC here and deleted the one appeared later. Now it is:

“Thus, we focused our study on the impacts of different scales of motion on source-specific equivalent BCs (eBCs), and we evaluated radiative effects of eBCs over a river-valley city.”

Line 81: I believe the authors meant: “the contributions of fossil fuel combustion and biomass burning to eBC concentrations”

Response: Yes, that is what we mean. Thanks for the comment, we have revised this sentence into

“The primary objectives of this study were: (1) to quantify the contributions of fossil fuel combustion and biomass burning to eBC concentrations, (2) to investigate the impacts of different scales of motion on the source-specific eBC, and (3) to estimate the radiative effects and the radiative efficiency of the source-specific eBC under different atmospheric motion scenarios.”

Method:

Line 88: Guanzhong Plain is where the river-valley city of Baoji is located, I guess? It would be nice to say so right at the beginning.

Response: We have revised this sentence to make that point clear. The revised paragraph can be seen in a response above to the general comments.

Section 2.1: a map of the region I think would help as figure 1.

Response: We have updated the map of the region in supplementary materials. The new map looks like:

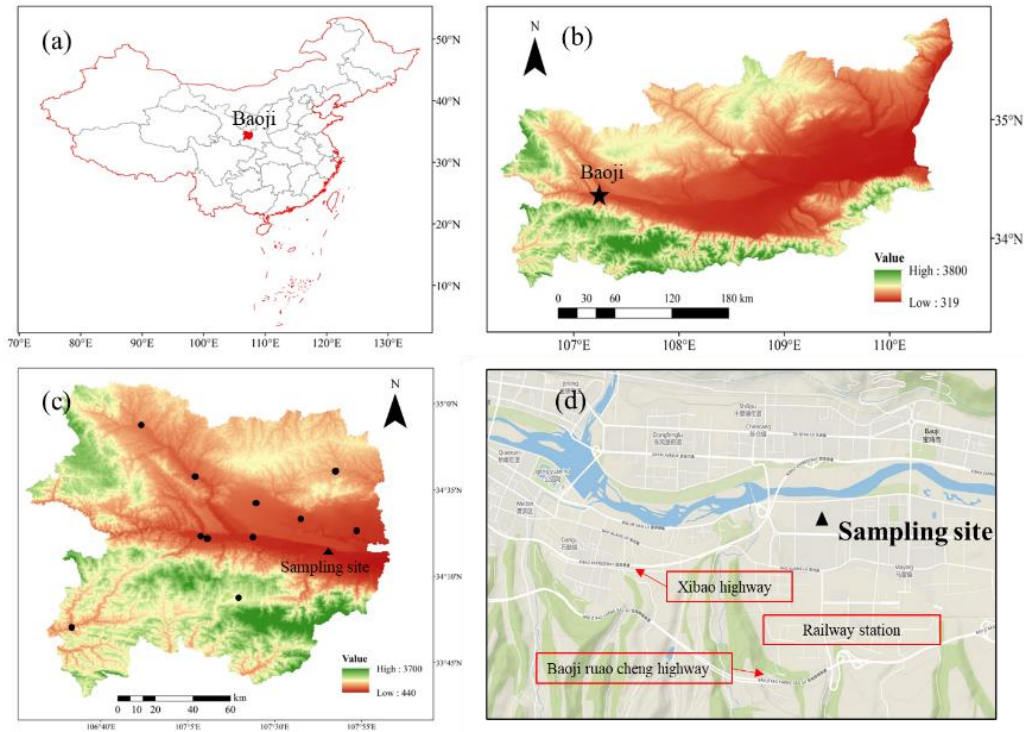


Figure R4. A map of the research site; (a) map of China—the red shape is the location of Baoji, (b) a map of the Guanzhong Plain, the black star represents the location of Baoji; (c) a map of Baoji City, the black dots and the black triangle represent 12 stations and the triangle is the location of sampling site, (d) a map of the sampling site.

Line 94: dense population, provide some numbers such as the total population, and population density.

Response: We have added the total population (0.341 million with 63.5% population living in downtown area) and population density (6003 people per km² in 2019) in the site description. The revised paragraph can be seen in the response above in the general comments.

Section 2.5 is quite confusing.

Response: We have revised this section and added more detailed explanations of the equation variables and had it edited by a native speaker for clarity. Now the section 2.5 reads:

“2.5 Indicators for the different scales of motion

The mathematical definitions of airflow condition proposed by Allwine and Whiteman (1994) were used in this study. The definitions quantify the flow features integrally at individual stations. Three variables were quantified, namely the actual wind run distance (S) which is the scalar displacement of the wind in 24 h (i.e. the accumulated distance of the wind), the resultant transport distance (L) which is the vector displacement of the wind in 24 h (i.e. the straight line from the starting point to the end point), and the recirculation factor (R) is based on the ratio of L and S which indicates the frequency of the wind veering in 24 h. The influences of different scales of atmospheric motions were assessed based on the method proposed by Levy et al., (2010), and for this, we used wind data at 100 m above the sampling site and the wind data from 12 monitoring stations at ground level (~15m) to indicate the different scales of motions. The winds at the surface monitoring stations were expected to be more sensitive to local-scale turbulence and convection than

the winds at 100 m. With less influence from the surface forces, the indicators at 100 m would be more sensitive to larger scales of motion. The equations used as follows:

$$L_{n\tau/bj} = T \left[\left(\sum_{j=i}^{i-\tau+1} u_i \right)^2 + \left(\sum_{j=i}^{i-\tau+1} v_i \right)^2 \right]^{1/2} \quad (11)$$

$$S_{n\tau/bj} = \sum_{j=i}^{i-\tau+1} (u_j^2 + v_j^2)^{1/2} \quad (12)$$

$$R_{n\tau/bj} = 1 - \frac{L_{i\tau}}{S_{i\tau}} \quad (13)$$

where T is the interval of the data (i.e., 60 min), i is the i^{th} the ending time step data, τ is the integration time period of the wind run (24 h), $i-\tau+1$ represents the data at the start time, and n is the number of monitoring stations (a total of 12 in this study). The quantities u and v are the wind vectors. Using the wind data from the 12 monitoring stations covering Baoji, the L and S values at the 12 different sites at ground level were calculated. $L_{n\tau}$ and $S_{n\tau}$ represent the resultant transport distance and the actual wind run distance at the n^{th} ($n = 1$ to 12) monitoring station at ground level; $R_{n\tau}$ is the recirculation factor at the n^{th} monitoring station which is calculated based on $L_{n\tau}$; and $S_{n\tau}$; L_{bj} , and S_{bj} are the resultant transport distance and the actual wind run distance at 100 m height above the ground. These represent the flow characteristics in higher atmosphere at the study site, and they were calculated by using the wind data at 100 m height. The recirculation factor (R_{bj}) was calculated for a height of 100 m.

As explained in Levy et al., (2010), if local-scale motions are strong and regional-scale motions are weak, the variations in winds at each station would not be likely to be uniform due to differences in local factors, and that would result in relatively large standard deviations (R_{std}) for $R_{n\tau}$. By contrast, if the local-scale motions are weak and the regional-scale motion is strong, the wind direction would be likely to be more uniform over a large area, and the R_{bj} and the R_{std} should be relatively smaller.”

Line 175: A ratio indicates a difference? That is confusing. Also, R is defined in 13 not as the ratio of L and S but as the ratio of the difference between S and L and S itself. Or is this a different R?

Response: We apologize for the inaccurate expression. The “R” on line 175 is the R defined in equation 13. We have corrected the description of the R in line 175. Now it consistent with the equation 13:

“Three variables were quantified, namely the actual wind run distance (S) which is the scalar displacement of the wind in 24 h (i.e. the accumulated distance of the wind), the resultant transport distance (L) which is the vector displacement of the wind in 24 h (i.e. the straight line from the starting point to the end point), and the recirculation factor (R) is based on the ratio of L and S which indicates the frequency of the wind veering in 24 h.”

Line 189: Again, if equation 13 is correct, then R is not the ratio of L to S but 1 – the ratio of L to S. Same for line 191 (which seems a repetition anyway).

Response: As noted above, we have corrected the expression that was on line 189 and 190, now it reads like:

“ $R_{n\tau}$ is the recirculation factor at the n^{th} monitoring station which is calculated based on $L_{n\tau}$ and $S_{n\tau}$; L_{bj} , and S_{bj} are the resultant transport distance and the actual wind run distance at 100 m height above the ground. These represent the flow characteristics in higher atmosphere at the study site, and they were calculated by using the wind data at 100 m height. The recirculation factor (R_{bj}) was calculated for a height of 100 m.”

Lines 192-193: this seems a bit of a circular argument (a tautology).

Response: We have rewritten this paragraph as follows:

“As explained in Levy et al., (2010), if local-scale motions are strong and regional-scale motions are weak, the variations in winds at each station would not be likely to be uniform due to differences in local factors, and that would result in relatively large standard deviations (R_{std}) for R_{nr} . By contrast, if the local-scale motions are weak and the regional-scale motions are strong, the wind direction would be likely to be more uniform over a large area, and the R_{bj} and the R_{std} should be relatively smaller.”

Line 207: provide a citation.

Response: We have provided the citation as following:

“Determining the size of the output map is crucial for SOM (Chang et al 2020 and Liu et al., 2021).”

Results and discussion:

Line 261: contain -> include

Response: Thanks for the correction, we have changed the word:

“The important input data included aerosol parameters, including aerosol optical depth (AOD), single scattering albedo (SSA), asymmetric factor (AF) and extinction efficiency, surface albedo, and atmospheric profile.”

Line 222: what is the default ratio in the model? And what model? OPAC?

Response: Yes, the model is OPAC. The default ratio used for converting mass concentration of BC to its number concentration is $5.99\text{E-}5$ ($\mu\text{g m}^{-3}/\text{part.cm}^{-3}$) in OPAC. To make this clear, we have added this information into the sentence to make it clear:

“The number concentrations of soot were derived from the mass concentrations of eBC with the default ratio ($5.99\text{E-}5$ $\mu\text{g m}^{-3}/\text{particle.cm}^{-3}$) in OPAC.”

Line 230: at -> of?

Response: We corrected this.

“where DRE_{eBC} is the DRE of source-specific eBC, $F\downarrow$ and $F\uparrow$ are the downward and upward flux, $DRE_{eBC,ATM}$ is the DRE of the source-specific eBC for the atmospheric column, that is, the DRE at the top of the atmosphere ($DRE_{eBC,TOA}$) minus that at the surface ($DRE_{eBC,SUF}$).”

Lines 238-239: Provide some more background or at least some references

Response: Thanks for the suggestion. We have added some background information about the Bootstrap (BS) and Displacement (DISP) with some references. Now it reads:

“Two diagnostic methods, Bootstrap (BS) and Displacement (DISP) (Norris et al, 2014; Brown et al. 2015) were used to validate the robustness and stability of the results. The BS method was used to assess the random errors and partially assess the effects of rotational ambiguity while DISP was used to evaluate rotational ambiguity errors. The results of the BS and DISP analyses showed that there was no swap for the 4-factor solution (Table S3).”

Line283: variations... varied... rephrase.

Response: We have corrected this awkward sentence:

“The results showed that eBC_{fossil} and $eBC_{biomass}$ were only weakly correlated ($r = 0.3$, Figure S9), indicating a reasonably good separation, and furthermore, their diel variations showed different patterns (Figure 2).”

Lines 293 – 294. Remove “New para here”

Response: We deleted it.

Line 295: why did the biomass burning increase after 6 pm? Is it indoor biomass burning for cooking or heating, or is it some other biomass burning?

Response: Based on previous research (Xie et al., 2010, Zhou et al., 2018) and what we know about residential energy usage in rural areas of Baoji, biomass is commonly used as fuel for residential cooking and heating. Therefore we believe that the biomass burning increased after 6 pm due to the evening meal preparation and residential heating.

To make this clear, we have revised this:

“In contrast, the diel variation of $eBC_{biomass}$ (Figure 2b) showed greater influences from meteorological conditions during the daytime, and $eBC_{biomass}$ showed lower concentrations during the day compared with the night. After 6 p.m., increased biomass burning from cooking and residential heating led to the emission of more $eBC_{biomass}$ and the stable PBLH hindered the dispersion of $eBC_{biomass}$; these two factors caused the $eBC_{biomass}$ to reach its peak at 8 p.m.”

Figure 3, caption: Explain the meaning of the gray and yellow areas even if that’s explained in the text.

Response: We added an explanation to the figure caption as follows:

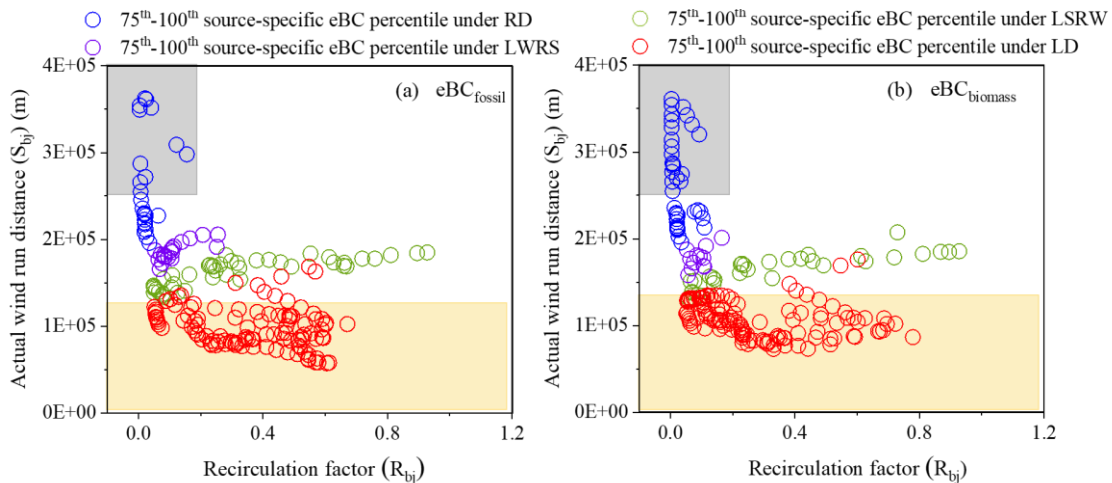


Figure R5. The 75th – 100th percentile mass concentrations of the eBC from fossil fuel combustion (eBC_{fossil}) and (b) the eBC from biomass burning ($eBC_{biomass}$) under local scale dominance (LD, red circle), local scale strong and regional scale weak (LSRW, green circle), local scale weak regional scale strong (LWRS, purple circle) and regional scale dominance (RD, blue circle). S_{bj} is actual wind run distance at 100m height, R_{bj} is the recirculation factor, the grey area indicates good ventilation ($S_{bj} \geq 250\text{km}$, $R_{bj} \leq 0.2$), the yellow area indicates air stagnation ($S_{bj} \leq 130\text{km}$).

Line 344: can one try to verify this with the backtrajectory analysis, or satellite products. etc.

Response: To verify the sources of eBC_{biomass} located further than that of eBC_{fossil} , we used non-parametric wind regression plots (Gu et al, 2020). As shown in the Figure R6, during the night, the eBC_{biomass} was higher when the wind speed was higher, while the eBC_{fossil} was higher when the winds were lower. This indicates that during night, the emission sources of eBC_{biomass} were located further than the sources for eBC_{fossil} , which explains why the mass concentrations of eBC_{biomass} did not decrease with the influence of regional-scale atmospheric motion increased. We have added this figure into the supplementary materials.

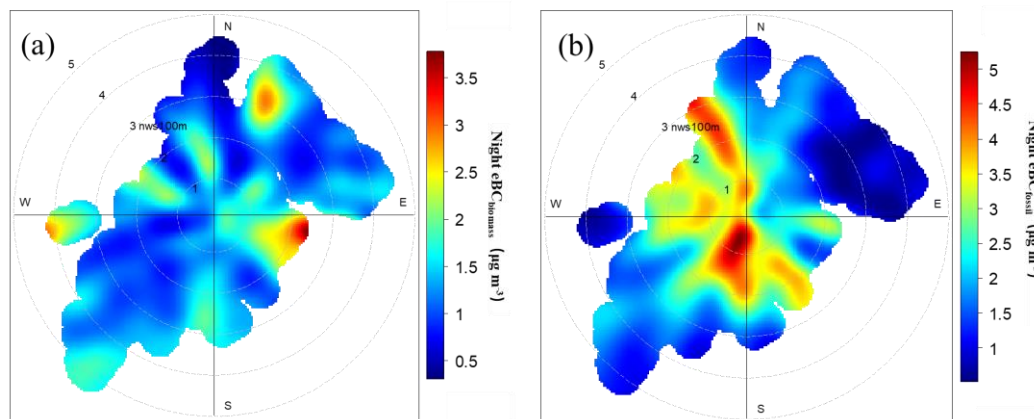


Figure R6 Non-parametric wind regression plots for eBC_{biomass} (a) and eBC_{fossil} (b) at night. The radial and tangential axes represent the wind direction ($^{\circ}$) and speed (m s^{-1}), respectively, nws100m represents the night wind speed 100m above the ground level.

Reference:

Gu, Y., Huang, R., Li, Y., et al., Chemical nature and sources of fine particles in urban Beijing: Seasonality and formation mechanisms, *Environmental International*, 140, 155732, <https://doi.org/10.1016/j.envint.2020.105732>, 2020

Line 350: I would suggest briefly summarizing what the angle distance clustering method is and how it works even if that's explained in detail in the cited paper.

Response: Thanks for the suggestion, we have added the detailed method explanation in the supplementary materials (Text S1) as shown in the response above. In the revised manuscript, the sentence reads like:

“To examine the impacts caused by air masses from different directions, the hourly 24h-back trajectories were calculated at 100 m above the ground using the Hybrid Single-Particle Lagrangian Integrated Trajectory model (Draxler and Hess, 1998, Text S2). Then the trajectories were clustered by using an angle-based distance statistics method (Text S2) to show the general directional features. This method determines the direction from which the air masses reach the site and has been widely used for air mass trajectory clusters. A detailed method description can be found in Sirois and Bottenheim (1995).”

Lines 360 – 362: Rephrase this sentence, there are several awkward readability issues.

Response: We have rewritten the sentence, now it reads:

“This could be attributed to more intensive emissions in the eastern parts of Baoji because 75% of the total

population of Baoji is located in this area (http://tjj.baoji.gov.cn/art/2020/10/15/art_9233_1216737.html, accessed on 25 September 2021, in Chinese).”

Line 360: remove “at” before “in”

Response: We apologize for this mistake, “at” has been removed from the sentence as shown in the response above.

Paragraph starting at line 405, specifically lines 411- 413: this is consistent with the higher MAC values.

Response: Yes, we agree. The higher DRE efficiencies can be attributed to the enhanced MAC of BC during the regional transport. So we have added the following text into the paragraph:

“Although $DRE_{eBC, ATM}$ declined with increased influences from the regional scale of motion, the $DRE_{eBC, ATM}$ efficiency ($DRE_{eBC, ATM}$ per mass concentration) was found to increase with greater regional-scale motion. Furthermore, the DRE efficiencies of both types of eBC under LD and LSRW were comparable, around 10 W m^{-2} (Table 2). In contrast, the efficiencies varied more when the regional-scale motions were stronger. Under LWRS, the efficiencies of eBC_{fossil} and $eBC_{biomass}$ were 13.5 ± 6.7 and 14.7 ± 8.1 (W m^{-2})/($\mu\text{g m}^{-3}$) respectively. Under RD, the efficiencies were even higher, 15.6 ± 8.9 (W m^{-2})/($\mu\text{g m}^{-3}$) for eBC_{fossil} and 15.5 ± 8.4 (W m^{-2})/($\mu\text{g m}^{-3}$) for $eBC_{biomass}$, which are > 1.5 times those recorded under LD. The higher eBC efficiencies may have been caused by the increases in the BC MAC during the regional transport. Studies have confirmed that the aging processes in the atmosphere can enhance the light-absorbing ability of BC (Chen et al., 2017; Shen et al., 2014), and regional transport can provide sufficient time for BC aging (Shiraiwa, et al. 2007; Cho et al., 2021).”

Caption of figure 5: explain what the different shadings represent. Also, x-axis label number four probably should be “DREeBCfossil, TOA” not “DREeBCbiomass, TOA”. It could be interesting to add another two panels with the equivalent calculations but in terms of efficiency to make more clear what is discussed in words in the paper.

Response: Thank you for pointing out this mistake. We have corrected the label and explained the shading and as suggested, we also added two figures. The figure has been replaced with following one:

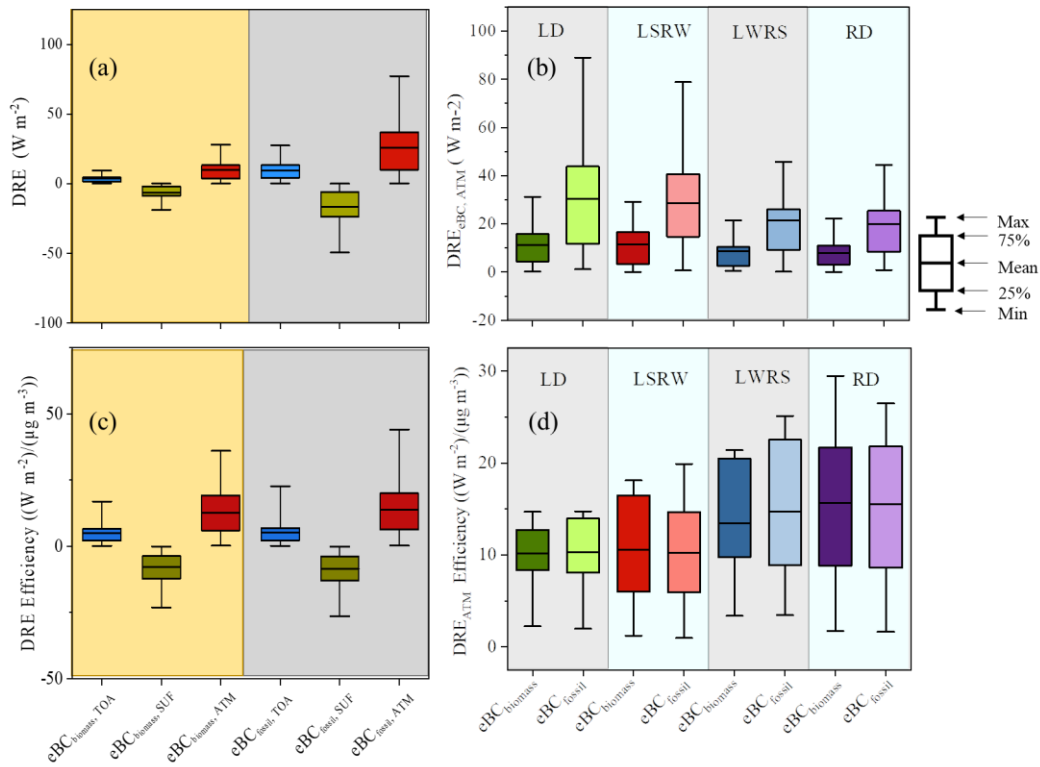


Figure R7. Direct radiative effect (DRE) of the eBC from fossil fuel combustion (eBC_{fossil}) shaded in grey and the eBC from biomass burning ($eBC_{biomass}$) shaded in yellow (a) in the top atmosphere (TOA), surface (SUF), and the atmosphere atmospheric column (ATM) and (b) the $DRE_{eBC,ATM}$ of two types of eBC under local scale dominance (LD) shaded in light grey labeled as LD, local scale strong and regional scale weak (LSRW) shaded in light blue labeled as LSRW, local scale weak regional scale strong (LWRS) shaded in light grey labeled with LWRS and regional scale dominance (RD) shaded in light blue labeled as RD (c) DRE efficiencies of $eBC_{biomass}$ (shaded in yellow) and eBC_{fossil} (shaded by grey) in TOA, SUF and ATM (d) DRE efficiencies of $eBC_{biomass}$ and eBC_{fossil} at ATM under LD (shaded in light grey labeled as LD), LSRW (shaded in light blue labeled as LSRW), LWRS (shaded in light grey labeled as LWRS) and RD (shaded in light blue labeled with RD).